Journal of Geophysical Research: Earth Surface

Supporting Information for

Anthropogenic Controls on Overwash Deposition: Evidence and Consequences

Laura J. Rogers[1], Laura J. Moore[1], Evan B. Goldstein[1], Christopher J. Hein[2], Jorge Lorenzo-Trueba[3], Andrew D. Ashton[4]

[1]: Department of Geological Sciences, University of North Carolina, Chapel Hill, NC 27599, United States
[2]: Department of Physical Sciences, Virginia Institute of Marine Science, College of William & Mary, Gloucester Point, VA 23062, United States
[3]: Department of Earth and Environmental Studies, Montclair State University, Montclair, NJ 07043, United States
[4]: Department of Geology and Geophysics, Woods Hole Oceanographic Institution, Woods Hole, MA 02543, United States

Contents of this file

Additional Supporting Information (Files uploaded separately)

None

Introduction

Supporting information includes additional analysis of error associated with LiDAR surveys collected by the US Geological Survey pre- and post-Hurricane Sandy (November, 2012). Analysis tests error induced by interpolation. Section 2 provides details of field observations collected from the Edwin B. Forsythe Wildlife Refuge, New Jersey (November of 2014). Data includes nine sediment cores and grain-size analysis of selected core samples. Grain size analysis was conducted using a Beckman Coulter LS 3 Series Laser Diffraction Particle Size Analyzer.

S1. Interpolation Induced Error Analysis

Triangulation methods are sensitive to the position of data points and the removal of points (as described in Section 3.1.2). Because the removal of points to assess accuracy results in increases in local point spacing, point removal to quantify induced error due to triangulation

likely provides an overestimate of actual error. QT Modeler's RMSE calculation provide an additional measure of error introduced by interpolation. After the gridding process is complete, QT Modeler calculates the RMSE of each 1 m grid square by comparing the original point cloud to the gridded surface without the actual removal of points. This resulted in a similar, yet smaller, induced error with a maximum RMSE of 0.054 m.

S2. Field Observations

To familiarize ourselves with the study area from the ground we compared the remotely-sensed LiDAR observations analyzed for this study with field observations. To accomplish this we collected cores and grab samples of surficial sediment from our natural area study site (the Edwin B. Forsythe Wildlife Refuge, Holgate, New Jersey) where overwash deposits were unlikely to have been disturbed by anthropogenic influences following Hurricane Sandy. Field sampling was done November 15-16, 2014, approximately two years after the LiDAR survey was completed November 1-5, 2012.

Within the area of interest, we selected eight cross-shore transects for sampling (Figure S2.1). We collected nine slide-hammer Geoprobe sediment cores samples (Figure S2.2), at designated locations. Sample locations were selected based on ground-penetrating radar (GPR) profiles collected concurrently using a Mala ProX with both 250 MHz and 500 MHz antennas. Cores were collected in 6 cm diameter polycarbonate liners within a stainless steel core barrel (Figure S2.2). Cores ranged from 65 cm to 175 cm in depth. Additionally, hand auger cores were collected at 25 m intervals along each of the eight transects with the intention to visually identify overwash layers in the field.

Cores were opened, described, photographed, and sampled at the University of North Carolina, Chapel Hill. Three representative cores are shown here (Figures S2.4 – S2.6). Based on visual inspection and with the intention to compare down-core changes in grain size with the extent of overwash, we selected three cores for detailed grain size analysis: BH123-2-2, BH105-5 and BH90-7, which are 90 m, 150 m and 200 m from the pre-storm MHW shoreline, respectively (Figure S2.7). We collected samples for grain size analysis at 15 cm intervals. Each sample was exposed to 600^0 C temperatures to remove organics, then analyzed using a Beckman Coulter LS 3 Series Laser Diffraction Particle Size Analyzer. The Wentworth scale was used to define general grain size classes. Given the large sampling interval of 15 cm, the overwash depths identified visually as described above are generally comparable to overwash depths identified using grain size analysis.

Comparison of overwash depths measured using LiDAR data with overwash depths measured in the sediment cores reveals general similarities but indicates that (as expected) changes have occurred due to natural beach processes in the intervening two years. We consider all cores in our comparison, except for core BH-105-4-2, which was accidentally collected below the depth of the base of the overwash signal we were attempting to capture (the overwash layer was estimated, based on LiDAR analysis, to begin at a depth of 49 cm, but we augered to a depth of 78 cm before collecting our core sample).

We measured overwash thickness in the cores as the distance between the ground surface and the first major lithologic contact (typically the contact between medium to coarse sand [overwash] and underlying peat). Comparison of overwash thickness measured in cores versus thicknesses derived from LiDAR observations yields absolute differences ranging from 2 to 40 cm, with an average absolute difference of 18 cm (Table S2 Figure S2.3). The sign of the differences is reflective of the patterns of morphological diagenesis associated with recovery (close to shore) and landward deflation due to aeolian transport and vegetation loss (Figure S2.3d) given that we sampled more than two years after Hurricane Sandy. Differences thus not only include errors arising from the LiDAR analysis but also volumetric changes in overwash

deposits that have occurred since deposition. For example, the two cores in which we measured overwash thicknesses of -28 and -24 cm relative to those derived from LiDAR are farthest from the shoreline, have limited vegetation due to overwash burial and are therefore vulnerable to erosion by wind. Additionally, the ground surface in these areas exhibited signs of deflation at the time of core collection; moreover, < 1m2 plots of land surrounding proximal vegetation clearly had amassed aeolian sediment. Consequently, significant aeolian reworking had occurred in the exposed, landward-most sections in the two years since Hurricane Sandy. Thus, this process of aeolian reworking and deflation reduced overwash thicknesses measured in these locations relative to the thicknesses measured using LiDAR observations.

We found similar post-storm morphologic changes documented on the seaward side of the island. The two cores we collected closest to the shoreline came from a zone in which recent accretion was apparent, likely via onshore ridge-and-runnel migration of bars. This resulted in field estimates of overwash deposition thickness substantially larger than those derived from the LiDAR analysis. These cores were also collected within a zone where the LiDAR analysis indicates alternation between erosional and accretional areas in close proximity, suggesting that positional error may also be affecting the accuracy with which comparison can be made at these cross-shore locations. Ultimately, differences between elevations extracted from LiDAR analysis and observations of overwash deposition in the field suggest considerable reworking in the two years since Hurricane Sandy impacted this area.

Figure S2.1

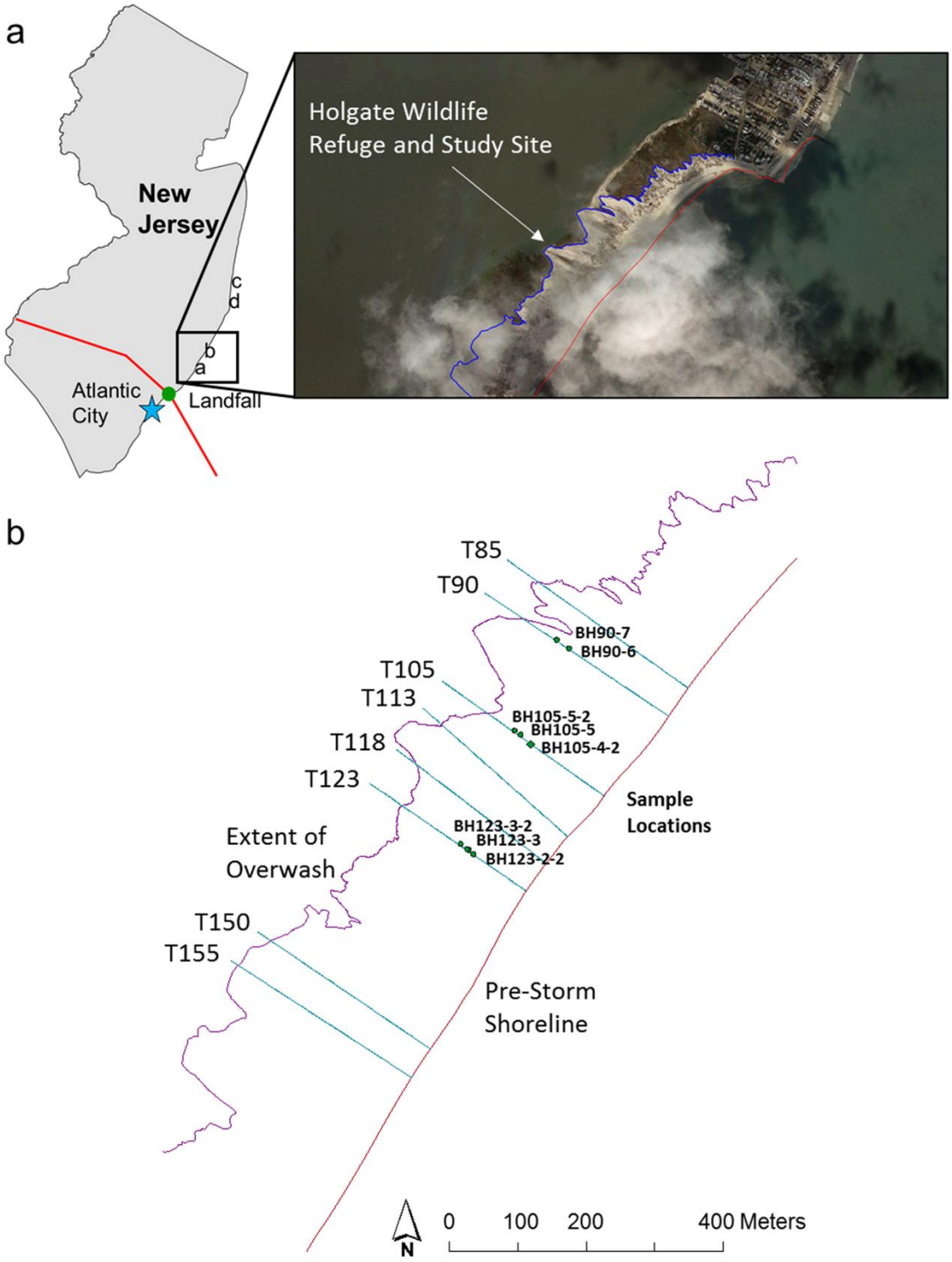

Figure S2.1. (a) Map of the study area relative to the path of the storm. The Edwin B. Forsythe Wildlife Refuge is located north of Atlantic City, NJ and is the location of our "natural" analysis site. (b) Location and naming of eight transects and sediment core locations. Image source: Google Earth.

Figure S2.2

Figure S2.2. Photos from the study site. (a) Slide-hammer Geoprobe core collection tools and methods. (b) and (c) Photos along Transect 90 looking west toward Barnegat Bay depicting vertical accretion occurring in the presence of vegetation and deflation occurring in the absence of vegetation.

Figure S2.3

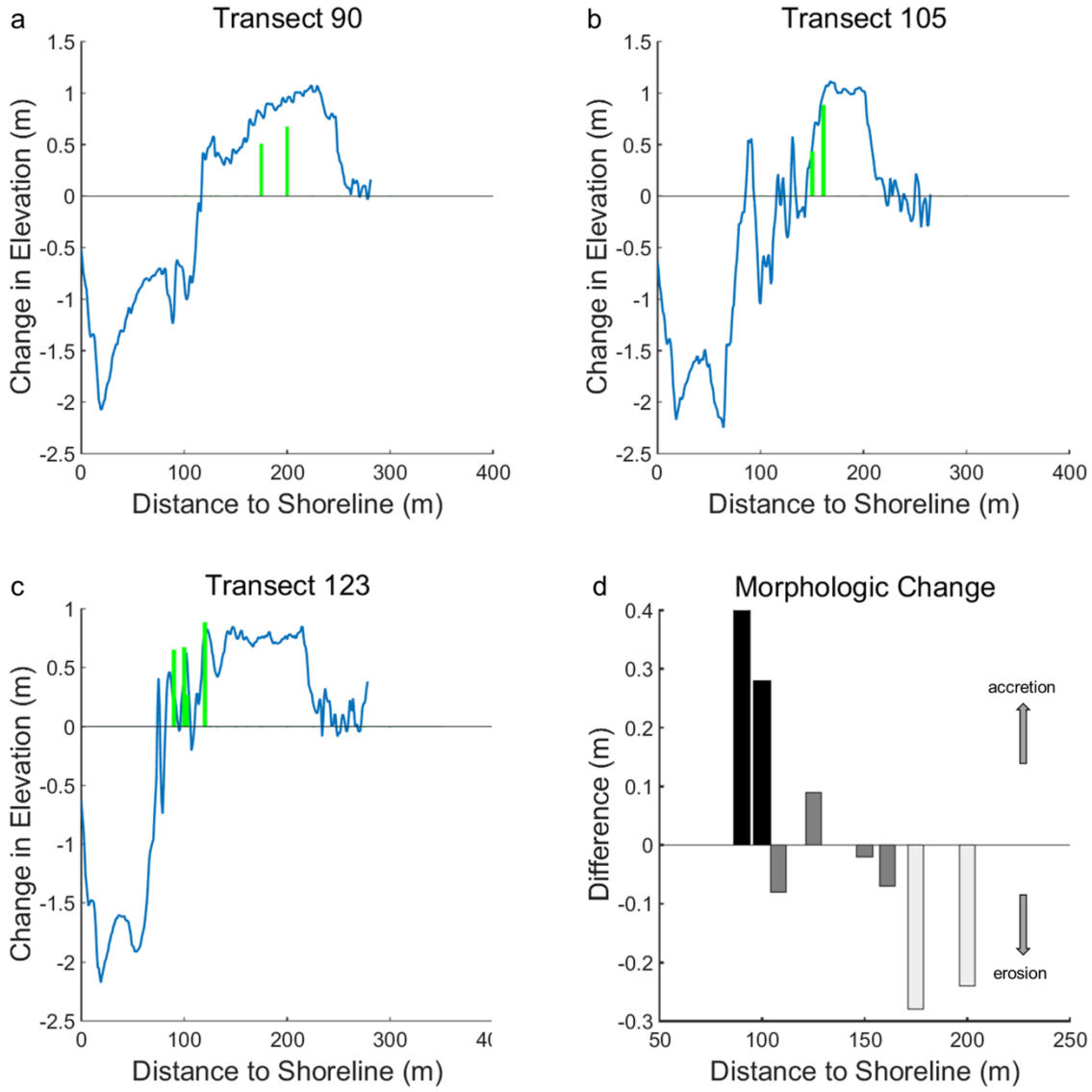

Figure S2.3. (a-c) LiDAR-derived elevation change profiles (blue lines) compared to overwash thicknesses identified in sediment cores (green lines). This comparison yields absolute differences ranging from 2 to 40 cm, with an average absolute difference of 18 cm. (d) The difference between LiDAR-derived overwash thickness and overwash thickness derived from cores illustrating morphologic change occurring between time of LiDAR surveys and sediment core collection – accretion nearest the shoreline and deflation toward the back-barrier bay.

Figure S2.4

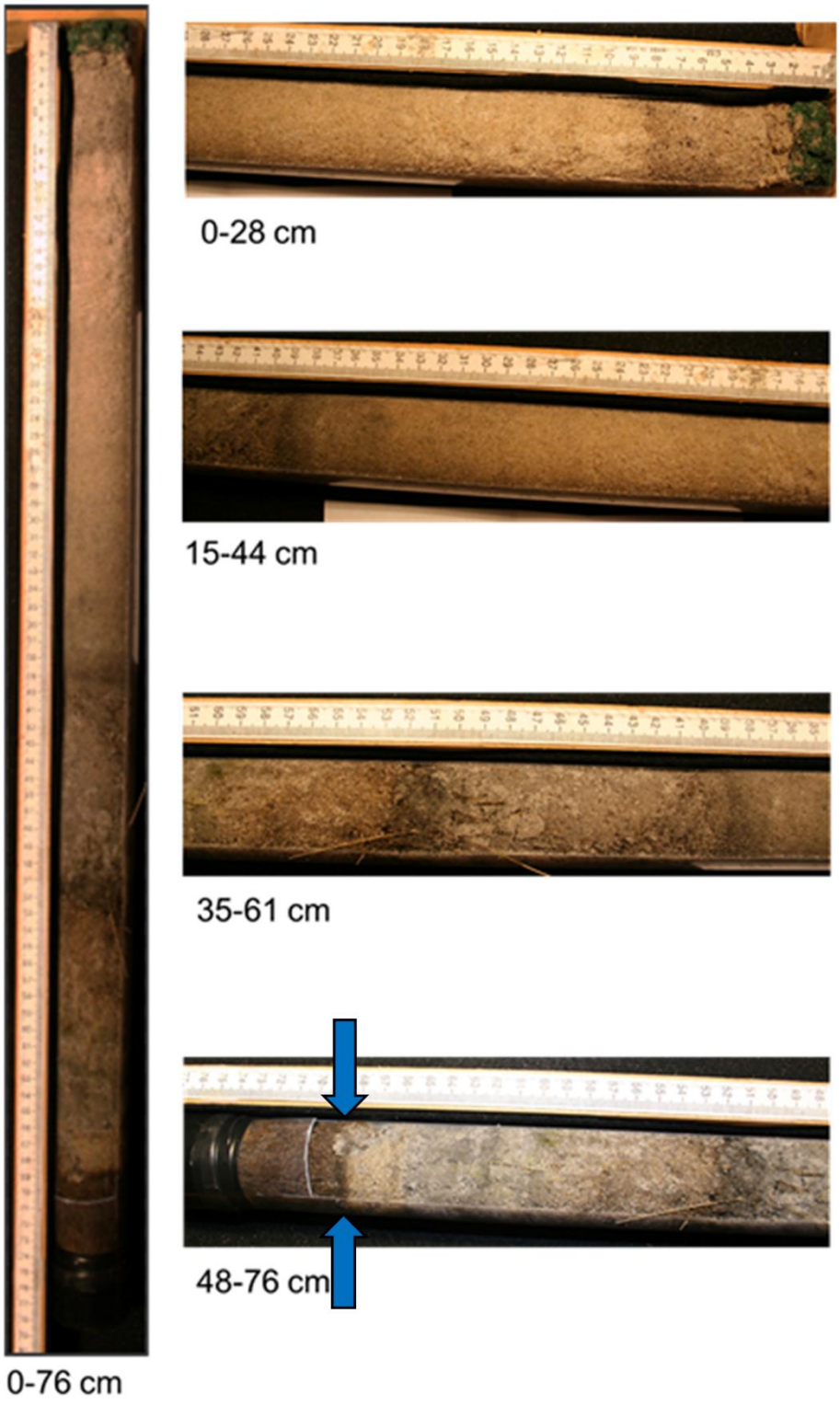

Figure S2.4. Core BH-90-7 (200 m from the shoreline). Overwash thickness (as measured by the first lithologic contact) 67 cm shown by blue arrows.

Figure S2.5

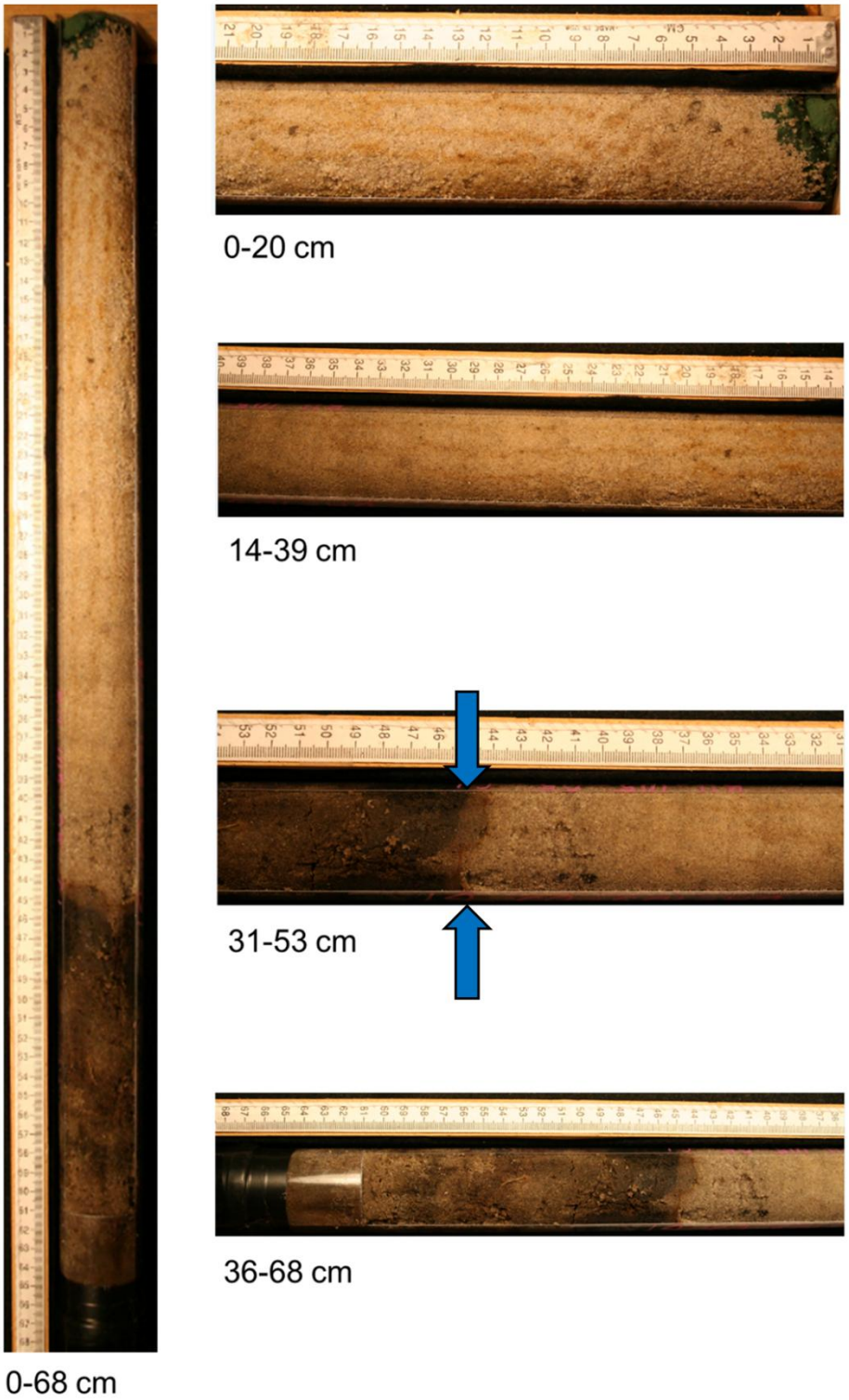

Figure S2.5. Core BH-105-5 (150 m from the shoreline). Overwash thickness (as measured by the first lithologic contact) 43 cm shown by blue arrows.

Figure S2.6

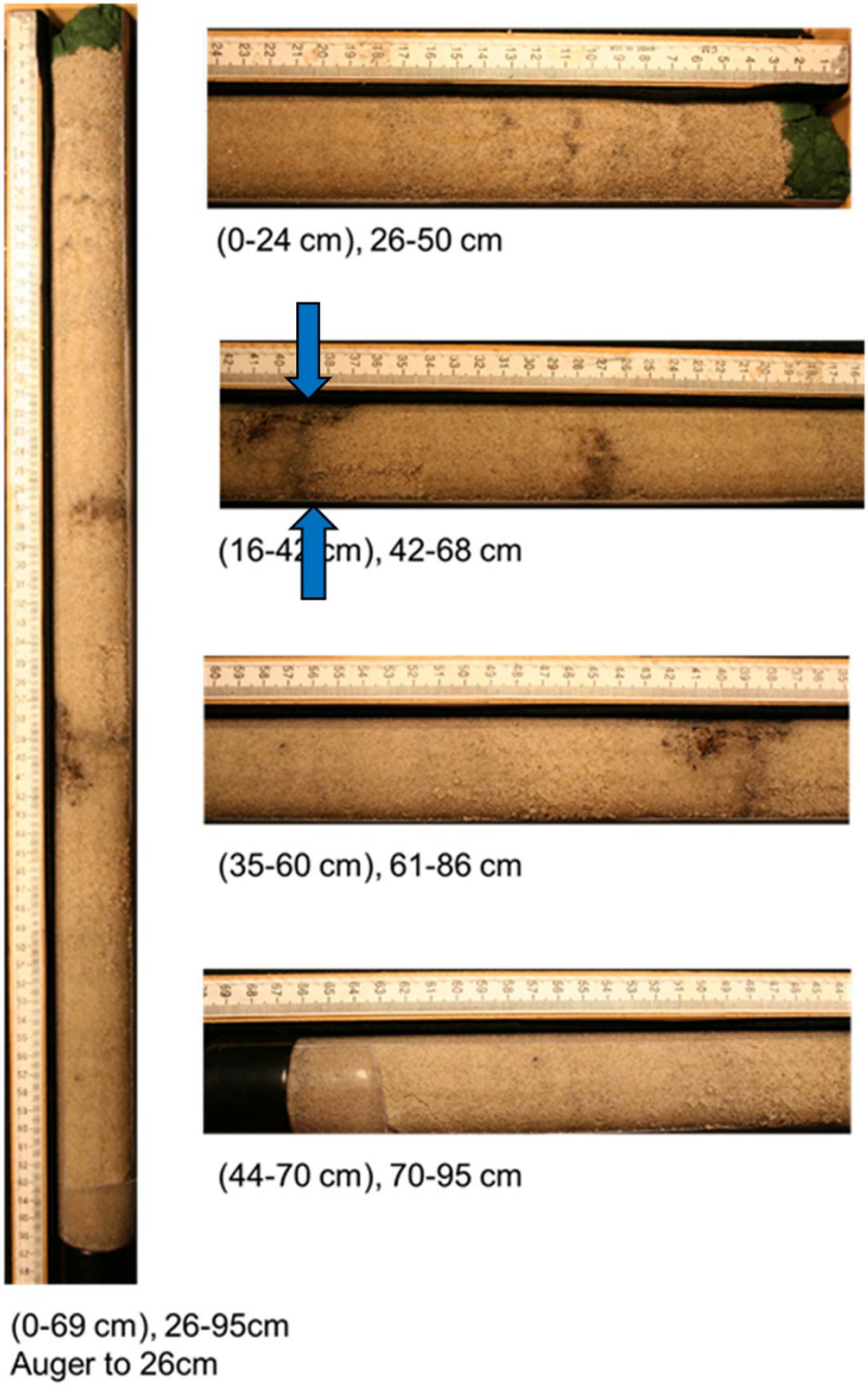

Figure S2.6. Core BH-123-2-2 (90 m from the shoreline). Overwash thickness (as measured by the first lithologic contact) 65 cm shown by blue arrows.

Figure S2.7

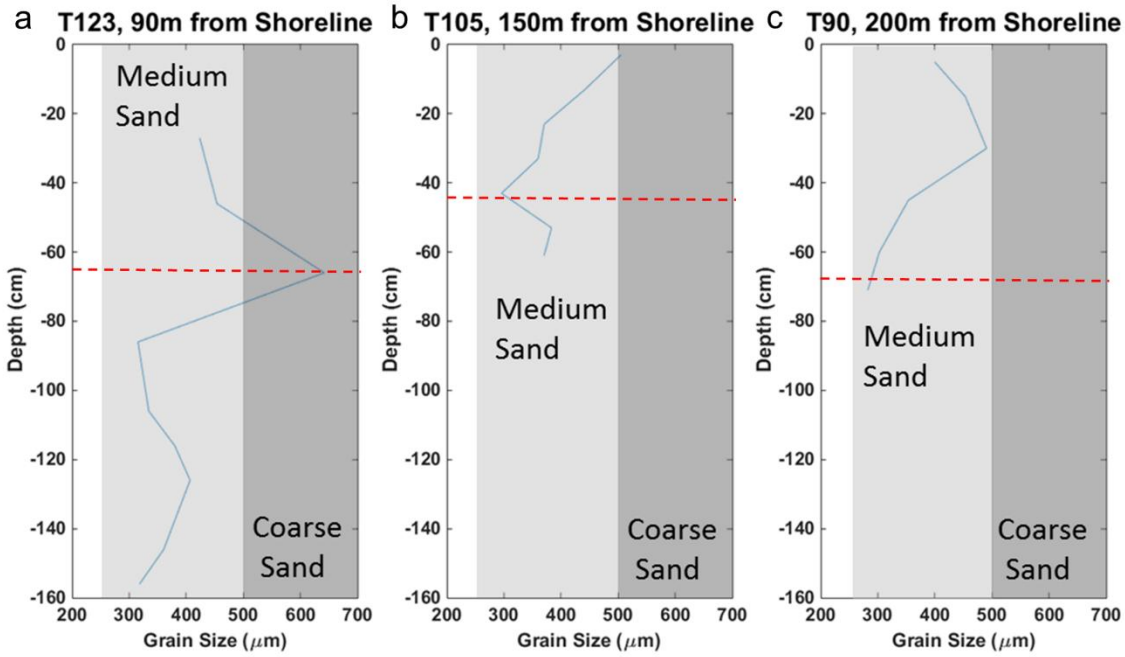

Figure S2.7. Results of grain size analysis conducted using a Beckman Coulter LS 3 Series particle size analyzer. Samples were analyzed at 15 cm intervals from three cores located at different distances from the shoreline. Grain size is categorized using the Wentworth Scale. Overwash thickness as identified visually is depicted as red dashed lines at (a) Core 123-2-2 (Figure S2.6) 65cm, (b) Core 105-5 (Figure S2.5) 43cm and (c) Core 90-7 (Figure S2.4) 67cm.

Table S2. Sediment core locations and overwash thickness comparisons

Core	Dist. to Shore (m)	Northing	Easting	Overwash Depth in Core (cm)	Overwash Depth from LiDAR (cm)	Diff. (cm)
90-6	175	4375769.32	562732.7499	50	78	-28
90-7	200	4375779.85	562714.5323	67	91	-24
105-4-2	133	4375635.87	562667.5412	126	49	-
105-5	150	4375640.61	562661.2974	43	45	-2
105-5-2	161	4375649.33	562653.2076	88	95	-7
123-2-2	90	4375468.65	562592.7106	65	25	+40
123-3	100	4375474.94	562585.7235	67	49	+28
123-3-2	103	4375476.04	562583.4492	27	35	-8
123-3-3	125	4375483.75	562574.1972	88	79	+9